Structure and Swelling of Grafted Polyelectrolytes: Predictions from a Nonlocal Density Functional Theory

Tao Jiang, Zhidong Li, and Jianzhong Wu*

Department of Chemical and Environmental Engineering, University of California, Riverside, California 92521

Received August 21, 2006; Revised Manuscript Received November 3, 2006

ABSTRACT: The properties of polyelectrolytes anchored on surfaces depend on a broad range of parameters including the characteristics of the polyions, salt concentration, ion valence, and solvent conditions. While these systems have been subjected to extensive theoretical and experimental investigations in particular in the brush limit, a number of important questions remain to be addressed concerning the electrostatic correlations and excluded-volume effects beyond typical mean-field approximations. In this work, we applied a nonlocal density functional theory (DFT) to tethered polyelectrolytes within a primitive model and examined the effects of salt concentration, polymer grafting density, and chain length on the polyion configurations, the mean electrostatic potential, and the distributions of both counterions and co-ions. Whereas the theoretical framework is directly applicable to arbitrary solution conditions, this work is focused on systems containing only monovalent ions so that the comparison can be made with the established results. Given the polyion chain length and grafting density, we predicted a smooth transition from the osmotic brush to the salted brush in response to the increase of the salt concentration. In the osmotic regime, the brush thickness is invariant with the salt concentration but grows with the grafting density. In the salted regime, the brush thickness follows the classical scaling relation $H \propto C_s^{-1/3}$ for long polyelectrolytes but noticeably, the magnitude of the fractional exponent declines as the polyion chain length falls. Linear relations between the polyelectrolyte chain length and the brush thickness were identified for both osmotic and salted brushes. Qualitatively, all these predictions were found in good agreement with experiments or with simulations.

1. Introduction

Polyelectrolyte brushes (PEBs) are charged polymers with one end grafted on a surface by either chemical or physical means.[1,2] In a chemically grafted PEB, the polymer ends are covalently bounded to the surface through chemical bonds.[3] Conversely, in a physically grafted PEB, attachment is often accomplished by copolymerization of the polyelectrolyte with a short hydrophobic chain at the end that provides sticky forces to the surface.[4,5] Over the past two decades, PEBs have received considerable research interest owed to their potential applications in colloidal stabilization,[6] surface protection,[7] and lubrication.[8,9]

The presence of long-range electrostatic interactions makes the properties of PEBs much more complicated than those corresponding to neutral polymer brushes. Since the pioneering works by Pincus[10] and by Borisov, Birshtein, and Zhulina,[11] numerous theoretical and experimental studies have been reported concerning the structure and surface properties of PEBs.[4,12−14] The theoretical investigations are primarily based on the scaling analyses and the self-consistent mean-field theories that rely on a number of simplifications.[10,11,15−18] For quenched PEBs, in which the number and positions of charges at each polymer chain are fixed, previous theoretical and experimental investigations have identified different brush regimes that depend on the PEB grafting density, degree of dissociation, and ionic strength.[10,17] Given the polyion chain length and grafting density, an increase in the salt concentration results in a transition from the osmotic brush to the salted brush. In the osmotic-brush regime, the counterions are mainly trapped inside the brush. In this regime, the scaling laws and self-consistent mean-field calculations predict that the brush thickness depends neither on the salt concentration nor on the polymer grafting density. In the salted-brush regime, it was predicted that the brush thickness scales with the grafting density by a power of 1/3 and with the salt concentration by a power of $-1/3$.[10,11]

Some recent experiments and simulations suggest that the scaling laws and the self-consistent mean-field theory might be insufficient to give a complete explanation of the swelling behavior of PEBs. For example, Romet-Lemonne etc.[5] and Ahrens etc.[19] found that, in the osmotic-brush regime, the brush thickness slightly increases with the grafting density. In addition, recent molecular dynamics simulations[19,20] corroborate the so-called "nonlinear osmotic-brush regime" identified by X-ray or neutron reflectivity measurements. It has been shown that the nonlinear osmotic-brush regime can be justified by a modified scaling theory taking into account the excluded-volume effects and the nonlinear elasticity of strongly stretched polymer chains.[19,20]

A number of molecular simulations have been reported concerning the swelling behavior and polyion distributions for PEBs. By using molecular dynamics (MD) simulations and a bead−spring model for polyions, Seidel and co-workers[19,20] suggested that in the osmotic regime, the brush thickness H depends weakly on the grafting density. With added salts, it follows a power law scaling $H \propto C_s^{-0.15}$ with the salt concentration C_s.[21] Chen and co-workers[22] used a lattice model for polyelectrolytes and a screened Coulombic potential for the electrostatic interactions and found that, as predicted by the scaling laws, with strong screening a PEB behaves like a neutral brush whereas with weak screening the brush thickness becomes a constant. More recently, Hehmeyer and Panagiotopoulos[23] performed lattice-based MC simulations but with explicit consideration of the electrostatic interactions due to small ions.

* Author to whom correspondence should be addresed. E-mail: jwu@engr.ucr.edu.

10.1021/ma061939t CCC: $37.00
Published on Web 12/20/2006

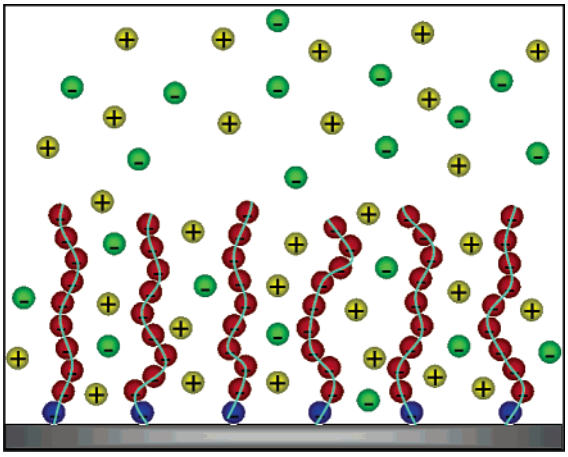

Figure 1. Schematic illustration of a primitive model for salted polyelectrolyte brushes (PEBs).

It was found that a PEB collapses at low temperature, maximizes its thickness at an intermediate temperature, and falls slowly as the temperature further rises. Because relatively short chains are used, the scaling laws are often not fully recovered by the simulation methods. Indeed, even within the simplified models, simulation of long-chain PEBs remains computationally challenging.

Density functional theory (DFT) provides an alternative method to simulations and to traditional mean-field theories by taking into account both short- and long-range correlations in a self-consistent manner.[24,25] In previous publications,[26,27] we have developed a nonlocal DFT for polyelectrolytes and tested its numerical performance by extensive comparisons with simulation results. In this work, we wish to extend the DFT to tethered polyelectrolyte layers by using a primitive model where the polyelectrolytes are modeled as tangentially connected charged-sphere chains, salt ions as monomeric charged spheres, and the solvent as a dielectric medium. We examine the effects of salt concentration, polyelectrolyte chain length, and grafting density on the swelling behavior by calculating the configurations of polyions and related ion distributions. The purposes of these calculations are two fold. First, molecular simulations of PEBs are mostly limited to relatively short chains but the scaling analyses and experiments are often concerned with long-chain polymers. A theoretical approach applicable to both regions will resolve some discrepancies identified in a number of previous investigations.[21] Second, the excluded-volume effects and long-range Coulomb correlations are often ignored in typical scaling analyses and mean-field calculations. By explicitly accounting for the polymer size and electrostatic correlations, DFT calculations are expected to provide deeper insights on how such effects influence the structure and swelling of PEBs.

The remainder of this article is organized as follows. Section 2 describes the molecular model and formulation of the DFT for tethered polyelectrolytes. In section 3, we investigate the effects of salt concentration, polyelectrolyte chain length, grafting density on the swelling of polyelectrolyte brushes and segmental density profiles in different brush regimes. Section 4 summarizes the main results and discussions.

2. Molecular Models and Density Functional Theory

We consider monodispersed polyions with one end grafted at a planar hard surface submerged in a good solvent containing monovalent counterions and co-ions, i.e., salt ions of the opposite or same charge of the polyions, respectively. Figure 1 shows a schematic representation of the primitive model for PEB systems. The grafted polyions are represented by freely jointed tangent chains of charged hard spheres with one end segment tethered to a neutral solid surface, salt ions are represented by charged hard spheres, and the solvent is a continuous medium of dielectric constant ϵ.

As in the primitive model for simple electrolyte solutions, the reduced interaction potential between any pair of charged spheres is given by

$$\beta u_{ij}(r) = \begin{cases} \infty, & r < \sigma_{ij} \\ l_B \dfrac{Z_i Z_j}{r}, & r \geq \sigma_{ij} \end{cases} \quad (1)$$

where r is the center-to-center distance, σ_k is the spherical diameter of particle k, $\sigma_{ij} = (\sigma_i + \sigma_j)/2$, Z_k is the valence, $\beta = 1/k_BT$ with k_B being the Boltzmann constant and T the absolute temperature. The Bjerrum length, $l_B = \beta e^2/\epsilon$, is chosen at 0.714 nm, corresponding to that for water at 298 K. We assume that the PEBs are in good solvent; i.e., attractions between polyelectrolyte segments are not considered.

Except the tethered segments, the surface energy for each sphere (a polyion segment or a small ion) is simply represented by a hard-wall potential

$$\beta\Psi_k(z) = \begin{cases} \infty, & z < \sigma_k/2 \\ 0, & z \geq \sigma_k/2 \end{cases} \quad (2)$$

where z is the perpendicular distance from the surface.

The Helmholtz energy functional can be expressed in terms of an ideal part corresponding to that of the polymers free of nonbonded interactions, and an excess accounting for nonbonded inter- and intramolecular interactions

$$F[\rho_M(\mathbf{R}), \{\rho_\alpha(\mathbf{r})\}] = F^{id}[\rho_M(\mathbf{R}), \{\rho_\alpha(\mathbf{r})\}] + F^{ex}[\rho_M(\mathbf{R}), \{\rho_\alpha(\mathbf{r})\}] \quad (3)$$

where $\mathbf{R} \equiv (\mathbf{r}_1,\mathbf{r}_2,...,\mathbf{r}_M)$ is a set of coordinates specifying the segmental positions of a polymer or the polyelectrolyte configuration, $\rho_M(\mathbf{R})$ stands for the multidimensional density profile of the polyelectrolyte chains as a function of configuration $\mathbf{R}$, $\rho_\alpha(\mathbf{r})$ is the density profiles of small ions.

The Helmholtz energy functional for noninteracting polymers is known exactly; it depends on the polymer configurations, the bond potential $V_b(\mathbf{R})$, and the density profiles of small ions:

$$\beta F^{id} = \int d\mathbf{R}\, \rho_M(\mathbf{R})[\ln \rho_M(\mathbf{R}) - 1] + \beta \int d\mathbf{R}\, \rho_M(\mathbf{R}) V_b(\mathbf{R}) + \sum_{\alpha=+,-} \int d\mathbf{r}\, \rho_\alpha(\mathbf{r})[\ln \rho_\alpha(\mathbf{r}) - 1] \quad (4)$$

For a freely jointed chain tethered at the surface, the bonding potential $V_b(\mathbf{R})$ is determined from

$$\exp[-\beta V_b(\mathbf{R})] = k\delta(z_1 - B) \prod_{i=1}^{M-1} \delta(|\mathbf{r}_{i+1} - \mathbf{r}_i| - \sigma_p) \quad (5)$$

where M stands for the degree of polymerization, δ is the Dirac-delta function, and k is a renormalization constant. The subscripts "p", "+", and "−" denote polyion segments, small cations, and anions, respectively. Throughout this work, we assume that the first segment of each polyion is tangentially grafted at the hard wall so that $B = \sigma_p/2$.

The expressions for the excess Helmholtz energies of polyelectrolytes have been reported in our previous publications.[26,27] But for clarity and for self-contained presentation of this work,

we recapitulate the key equations. Within the primitive model, the excess Helmholtz energy functional for PEBs can be expressed as a summation of the excluded-volume effects and charge/chain correlations

$$F^{ex} = F^{ex}_{hs} + F^{ex}_{ch} + F^{ex}_{C} + F^{ex}_{el} \tag{6}$$

where F^{ex}_{hs}, F^{ex}_{ch}, F^{ex}_{C}, and F^{ex}_{el} represent the excess Helmholtz energy functional due to the hard-sphere repulsions, the chain connectivity, the direct Coulomb energy, and the electrostatic correlations, respectively.

The excess Helmholtz energy functional due to the hard-sphere repulsion, F^{ex}_{hs}, can be accurately described by a modified fundamental measure theory (MFMT)[28,29]

$$\beta F^{ex}_{hs} = \int \Phi^{hs}[n_\omega(\mathbf{r})]\, d\mathbf{r} \tag{7}$$

in which the reduced excess energy density Φ^{hs} is a function of six weighted densities $n_\omega(\mathbf{r})$[30]

$$\Phi^{hs} = -n_0 \ln(1-n_3) + \frac{n_1 n_2 - \mathbf{n_{V1}}\mathbf{n_{V2}}}{1-n_3} + \frac{1}{36\pi}\left[n_3 \ln(1-n_3) + \frac{{n_3}^2}{(1-n_3)^2}\right]\frac{({n_2}^3 - 3n_2\mathbf{n_{V2}}\mathbf{n_{V2}})}{{n_3}^3} \tag{8}$$

According to an extension of the first-order thermodynamic perturbation theory (TPT1),[31] the excess Helmholtz energy functional for chain connectivity F^{ex}_{ch} can also be expressed in terms of the weighted densities

$$\beta F^{ex}_{ch} = \frac{1-M}{M}\int n_{0p}\zeta_p \ln y(\sigma_p, n_\omega)\, d\mathbf{r} \tag{9}$$

where M is the polymer chain length, $\zeta_p = 1 - (\mathbf{n_{V2p}}\mathbf{n_{V2p}})/{n_{2p}}^2$, and $y(\sigma_p, n_\omega)$ stands for the contact value of the cavity correlation function (CCF) of the polymer segments when they are disconnected (i.e., in a solution of monomeric charged spheres)[32,33]

$$y(\sigma_p, n_\omega) = \left[\frac{1}{1-n_3} + \frac{n_2\sigma_p(1 - \mathbf{n_{V2}}\mathbf{n_{V2}}/{\mathbf{n}_2}^2)}{4(1-n_3)^2}\right] \exp\left(-\frac{\Gamma^2 {a_p}^2}{4\pi^2 l_B \sigma_p}\right)\exp\left(\frac{l_B {Z_p}^2}{\sigma_p}\right) \tag{10}$$

Similar to the thermodynamic perturbation theory of bulk polyelectrolyte solutions,[32,33] the parameters Γ and a_p can be calculated from

$$\Gamma = \sqrt{\pi l_B \sum_{k=p,+,-} n_{0k}\left(\frac{1}{1+\Gamma\sigma_k}\right)^2\left(Z_k - \frac{\pi P_n {\sigma_k}^2}{2(1-n_3)}\right)^2} \tag{11}$$

$$a_p = \frac{2\pi l_B\left(Z_p - \frac{\pi P_n {\sigma_p}^2}{2(1-n_3)}\right)}{\Gamma(1+\Gamma\sigma_p)} \tag{12}$$

with

$$P_n = \sum_{k=p,+,-}\frac{2n_{1k}Z_k}{1+\Gamma\sigma_k}\Big/\left(1 + \frac{3}{(1-n_3)}\sum_{k=p,+,-}\frac{n_{3k}}{1+\Gamma\sigma_k}\right) \tag{13}$$

The excess Helmholtz energy functional for the chain connectivity takes into account the effect of bond connection on the intramolecular correlations, which is different from the direct bonding potential considered in the ideal-gas term.

The direct Coulomb term F^{ex}_{C} is known exactly

$$\beta F^{ex}_{C} = \frac{l_B}{2}\sum_{i,j=p,+,-}\int\int d\mathbf{r}\, d\mathbf{r}'\frac{Z_i Z_j \rho_i(\mathbf{r})\rho_j(\mathbf{r}')}{|\mathbf{r}-\mathbf{r}'|} \tag{14}$$

Because the bulk solution is free of polyions, the Helmholtz energy functional F^{ex}_{el} due to the electrostatic correlations can be approximated by a quadratic functional Taylor expansion with respect to the bulk densities of small ions $\{\rho^b_\alpha\}$[34]

$$\beta F^{ex}_{el} = \beta F^{ex}_{el}[\{\rho^b_\alpha\}] - \int d\mathbf{r}\sum_{i=+,-}\Delta C^{(1)el}_i(\rho_i(\mathbf{r}) - \rho^b_i) - \frac{1}{2}\int\int d\mathbf{r}\, d\mathbf{r}'\sum_{i,j=+,-}\Delta C^{(2)el}_{ij}(|\mathbf{r}-\mathbf{r}'|)(\rho_i(\mathbf{r}) - \rho^b_i)(\rho_j(\mathbf{r}') - \rho^b_j) \tag{15}$$

where the residual first-order and second-order direct correlation functions (DCF) are defined as, respectively,

$$\Delta C^{(1)el}_i = -\beta\mu^{el}_i = -\delta\beta F^{ex}_{el}/\delta\rho_i(\mathbf{r})|_b \tag{16}$$

$$\Delta C^{(2)el}_{ij}(|\mathbf{r}-\mathbf{r}'|) = -\delta^2\beta F^{ex}_{el}/\delta\rho_i(\mathbf{r})\delta\rho_j(\mathbf{r}')|_b \tag{17}$$

In this work, $\Delta C^{(2)el}_{ij}(r)$ is obtained analytically from the mean-spherical approximation (MSA) for simple electrolytes[35,36]

$$\Delta C^{(2)el}_{ij}(r) = C_{ij}(r) + \frac{l_B Z_i Z_j}{r} - C^{hs}_{ij}(r) \tag{18}$$

where the three terms on the right side represent the total two-body direct correlation function and that from contributions of electrostatic and hard sphere interactions.

The density profiles for polyelectrolyte segments and for salt ions are solved by minimizing the grand potential

$$\Omega[\rho_M(\mathbf{R}), \{\rho_\alpha(\mathbf{r})\}] = F[\rho_M(\mathbf{R}), \{\rho_\alpha(\mathbf{r})\}] + \int[\Psi_M(\mathbf{R}) - \mu_M]\rho_M(\mathbf{R})\, d\mathbf{R} + \sum_{\alpha=+,-}\int d\mathbf{r}\,\rho_\alpha(\mathbf{r})[\Psi_\alpha(\mathbf{r}) - \mu_\alpha] \tag{19}$$

where $d\mathbf{R} = d\mathbf{r}_1 d\mathbf{r}_2 \cdots d\mathbf{r}_M$ represents a set of differential volumes, and μ_M and μ_α are the chemical potentials of polyions and small ions respectively. The external potential of polyions $\Psi_M(\mathbf{R})$ applies to individual segments, i.e., $\Psi_M(\mathbf{R}) = \sum_{i=1}^{M}\Psi_p(\mathbf{r}_i)$, where $\Psi_p(\mathbf{r}_i)$ is the external potential on individual segments, and $\Psi_\alpha(\mathbf{r})$ is the external potential for small ions.

Minimization of the grand potential yields a set of Euler−Lagrange equations for the density profiles of polyion chains and small ions:

$$\rho_M(\mathbf{R}) = \exp\left\{\beta\mu_M - \beta V_b(\mathbf{R}) - \sum_{i=1}^{M}\left[\beta\Psi_p(\mathbf{r}_i) + \frac{\delta\beta F^{ex}}{\delta\rho_p(\mathbf{r}_i)}\right]\right\} \tag{20}$$

$$\rho_\alpha(\mathbf{r}) = \exp\left[\beta\mu_\alpha - \beta\Psi_\alpha(\mathbf{r}) - \frac{\delta\beta F^{ex}}{\delta\rho_\alpha(\mathbf{r})}\right] \tag{21}$$

Once we have the polymer density profiles, the overall segment density of polyions can be determined from

$$\rho_p(\mathbf{r}) = \sum_{i=1}^{M} \rho_{si}(\mathbf{r}) = \sum_{i=1}^{M} \int d\mathbf{R}\, \delta(\mathbf{r} - \mathbf{r}_i)\rho_M(\mathbf{R}) \quad (22)$$

where $\rho_{si}(\mathbf{r})$ stands for the local density of segment i.

For systems with the density distributions changing only in z-direction, eqs 21 and 22 can be simplified to[31]

$$\rho_\alpha(z) = \exp\left[\beta\mu_\alpha - \beta\Psi_\alpha(z) - \frac{\delta\beta F^{ex}}{\delta\rho_\alpha(z)}\right] \quad (23)$$

$$\rho_p(z) = k\exp(\beta\mu_M)\sum_{i=1}^{M}\exp[-\beta\lambda_p(z)]G_L^i(z)G_R^i(z) \quad (24)$$

with $\lambda_p(z) = \delta F_{ex}/\delta\rho_p(z) + \Psi_p(z)$. The propagator functions $G_L^i(z)$ and $G_R^i(z)$ arise from the connection of the polymer segments due to the direct bonding potential. These functions are equivalent to the Green functions used in a typical polymer self-consistent-field theory.[37] In this work, the propagator functions are determined from the recurrence relations

$$G_L^i(z) = 2\pi\sigma_p\int dz'\exp[-\beta\lambda_p(z')]\theta(\sigma_p - |z - z'|)G_L^{i-1}(z') \quad (25)$$

for $i = 3, ..., M$ with

$$G_L^{\,2}(z) = 2\pi\sigma_p\exp\left[-\beta\lambda_p\left(\frac{\sigma_p}{2}\right)\right]\theta\left(\sigma_p - \left|z - \frac{\sigma_p}{2}\right|\right) \quad (26)$$

and

$$G_R^i(z) = 2\pi\sigma_p\int dz'\exp[-\beta\lambda_p(z')]\theta(\sigma_p - |z - z'|)G_R^{i+1}(z') \quad (27)$$

for $i = 1, ..., M - 1$ with $G_R^M(z) = 1$.

Finally, the density distribution of the first segments is given by

$$\rho_{s1}(z) = \rho_g\delta\left(z - \frac{\sigma_p}{2}\right) \quad (28)$$

where ρ_g is the grafted density defined as the number of polyions per unit surface area. The constant $k\exp(\beta\mu_M)$ in eq 24 is determined by normalization conditions applied to each segment, i.e., $\int\rho_{si}(z)\,dz = \rho_g$ for $i = 2, ..., M$.

For more efficient computation of the density profiles of charged species, we define the mean electrostatic potential

$$Z_k e\psi(\mathbf{r}) = \Psi_k^C(\mathbf{r}) + \frac{\delta F_C^{ex}}{\delta\rho_k(\mathbf{r})} \quad (29)$$

where the first term on the right side is the electrostatic potential due to the surface charge which is assumed to be zero in this work for a neutral surface, and the second term arises from the interactions among mobile charges. For the systems considered in this work, $\psi(\mathbf{r})$is given by

$$\psi^*(z) \equiv \beta e\psi(z) = 4\pi l_B\int_z^\infty dz'(z - z')\sum_{k=p,+,-} Z_k\rho_k(z') \quad (30)$$

The density distributions of polyion segments, cations and anions satisfy the electroneutrality condition

$$\int_0^\infty dz'\sum_{k=p,+,-} Z_k e\rho_k(z') + Q = 0 \quad (31)$$

where Q is the surface charge density. Throughout this work, we assume $Q = 0$, i.e., all brushes are tethered to a neutral surface.

The density profiles of polyion segments and small ions are solved by using the conventional Picard iteration method. The iteration starts with the bulk densities for the density profiles of small salt ions. The density profiles of polyion segment are calculated from the salt density profiles and the PEB grafting density. During each iteration, the effective field

$$\lambda_k(z) = \frac{\delta F_{ex}}{\delta\rho_k(z)} + \Psi_k(z) \quad (32)$$

and the recurrence functions $G^i(z)$ are calculated and from which we obtain a new set of density profiles by using eqs 23 and 24. The new density profiles are then mixed with the previous results to give the next inputs. The final results are achieved when the overall difference between input and output density profiles is less than 1×10^{-6}. Once we get the density profiles of polyion segments, the reduced thickness of the PEB, H, is calculated from the first moment of the polyion segment density profile

$$H = \frac{2\int_0^\infty z\rho_p(z)\,dz}{\int_0^\infty \rho_p(z)\,dz} \quad (33)$$

3. Results and Discussion

3.1. Effect of Salt Concentration on the Brush Thickness. The DFT outlined above is directly applicable to systems with multivalent ions. However, for comparison with established results, we consider only monovalent ions in the following discussions. To minimize the number of unknown parameters, we use the same diameter ($\sigma = 0.425$ nm) for the counterions, co-ions, and polyion segments. Each counterion bears a negative charge, and each co-ion or polyion segment has one positive charge. A similar model was used by Patra et al. in studying the adsorption of polyelectrolytes on oppositely charged surfaces.[38] In the previous publications,[26,27] we found that in comparison with the electrostatic effects, the segment size has a relatively small effect on the interfacial behavior of polyelectrolytes. We expect that the hypothesis of equal size for polymer segments and small ions will not change the major conclusions of this work.

Figure 2 presents the calculated brush thicknesses for three PEBs with the chain lengths equal to $M = 20$, 50, and 100. In these calculations, the grafting density of polyelectrolytes is fixed at $\rho_g\sigma^2 = 10^{-2}$ while the salt concentration varies from $\rho_s\sigma^3 = 10^{-4}$ to 10^{-1}. The graph is plotted in logarithm scales for easy identification of the scaling relations. At a given chain length, the brush thickness is essentially a constant when the salt concentration increases from $\rho_s\sigma^3 = 10^{-4}$ to 10^{-3}. The invariance of brush thickness at the low salt concentration is known as the osmotic-brush regime defined first by Pincus[10] and by Borisov and co-workers.[11] The osmotic-brush regime has been confirmed by a number of theoretical calculations and by experiments.[4,14] At high salt concentrations ($\rho_s\sigma^3 > 10^{-2}$), Figure 2 shows a power-law behavior for the brush thickness, which is referred to as the salted-brush regime by Pincus and others.[10,11] In this regime, it is well-established that the brush thickness follows the scaling relation $H \propto \rho_s^{-1/3}$, shown as a dashed line in Figure 2.

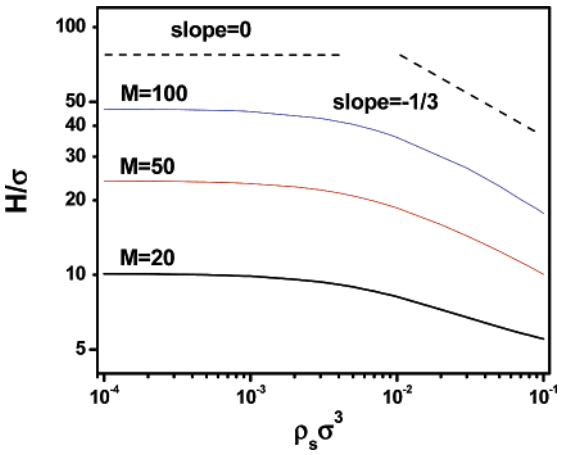

Figure 2. Dependence of the brush thickness on salt concentration for chain length $M = 20$, 50, 100. Here the reduced grafting density is $\rho_g\sigma^2 = 10^{-2}$. Dashed lines are predictions of the scaling laws for the salted and osmotic brushes.

While the DFT calculations confirm similar scaling relations for long polyelectrolyte chains (the slopes for $M = 50$ and 100 are -0.31 and -0.35, respectively), the fractional exponent noticeably decreases with the chain length for short chains. For $M = 20$, the mean separation between tethered polyelectrolytes is slightly larger than the polyelectrolyte size. With the increase of the salt concentration, the grafted polyelectrolyte chains undergo a transition from the osmotic sticks to salted coils. In the later case, the brush thickness scales as $H \propto \rho_s^{-0.17}$, which is in excellent agreement with the theoretical prediction by Borisov et al.[17] The scaling behavior was also confirmed by recent experiments for PSS adsorbed on a bare mica surface,[39] and by MD simulations[21] for relatively short PEBs in the present of salt (with chain length $M = 30$ in a monovalent electrolyte solution, $H \propto \rho_s^{-0.15}$). Figure 2 suggests that even for relatively short chains, the dependence of grafted layer thickness on the effect of salt concentration can be faithfully captured by the DFT. Moreover, DFT is able to bridge the gap between the scaling analysis for long polyelectrolyte chains and simulations for relatively short chains and reproduce the correct results in both limits. Figure 2 shows a smooth transition from the osmotic-brush regime to the salted-brush regime. The transition occurs approximately at $\rho_s\sigma^3 = 10^{-3}$–10^{-2}, relatively insensitive to the chain length.

Figure 3 presents the density profiles of polyion segments and salt ions at four different salt concentrations, $\rho_s\sigma^3 = 10^{-4}$, 10^{-3}, 10^{-2}, and 10^{-1}. Here the polyion chain length is $M = 50$ and the grafting density is the same as that used in Figure 2. Approximately, parts a and b of Figure 3 correspond to situations in the osmotic-brush regime, Figure 3c is for the transition region, and Figure 3d is for the salted-brush region. Unlike a typical mean-field theory, DFT is able to capture the oscillations of the density profiles near the surface owed to the chain connectivity and the excluded volume effects. Similar density profiles were identified by molecular simulations.[21] The first peak appears at 1.5σ, primarily due to the density of the segments immediately connected to the tethered segments, and the other peaks correspond to the densities of consecutive segments. The chain-connection effect is most apparent for the extended polyions, and it diminishes quickly at high salt concentrations due to the excluded-volume effects and probably to a less extent, electrostatic interactions. At high salt concentrations, the density distribution resembles a parabolic profile as in a typical neutral brush.[40,41] At low salt concentrations,

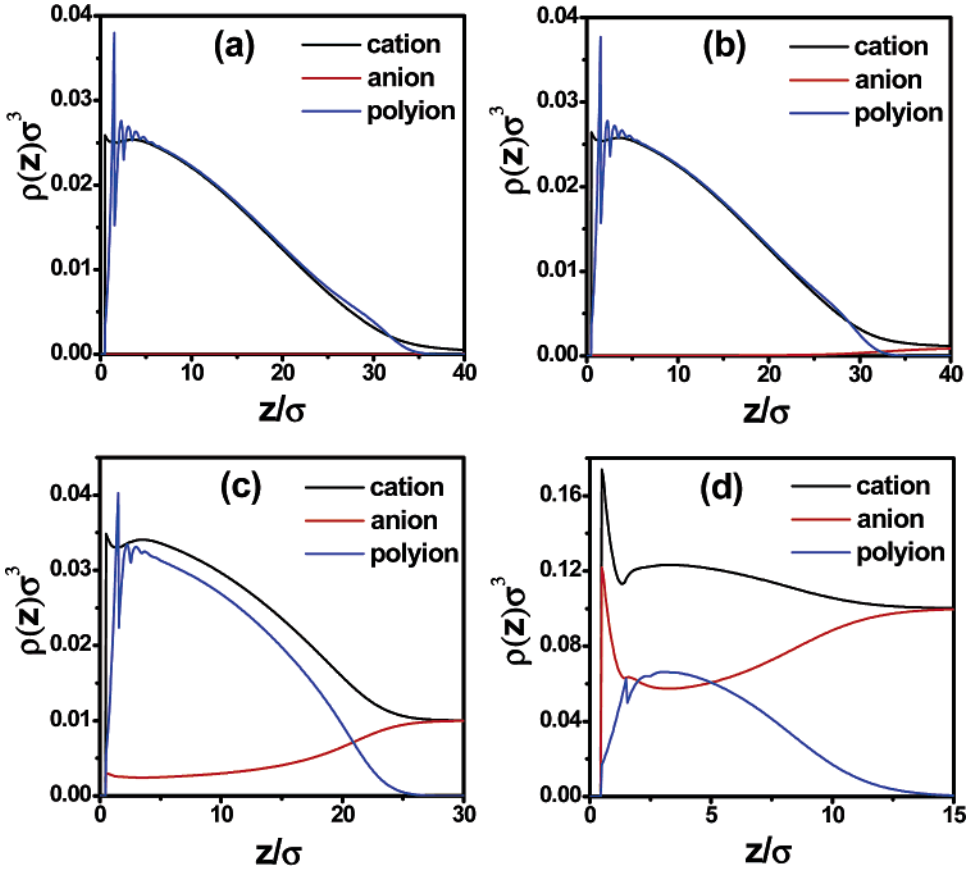

Figure 3. Density profiles of polyions ($M = 50$), cations and anions: (a) $\rho_s\sigma^3 = 10^{-4}$; (b) $\rho_s\sigma^3 = 10^{-3}$; (c) $\rho_s\sigma^3 = 10^{-2}$; (d) $\rho_s\sigma^3 = 10^{-1}$. The grafting density is the same as that appearing in Figure 2.

however, the density profile of polyion segments exhibits a long "tail" and thus is different from that for neutral brushes.

Figure 3a indicates that the counterion concentration closely follows that of the polyion segments, suggesting a neutralization of the polyion backbone as predicted by Manning's theory. However, near the tethering surfaces, the counterion concentration does not exhibit strong oscillation as shown in the density profile of polyion segments. Significant deviation is also apparent near the brush rim. Whereas the counterions are mostly trapped inside the polyelectrolyte brush and the concentration of co-ions in the osmotic-brush regime is negligible, the distributions of both polyion segments and counterions within the brush are highly inhomogeneous.

Figure 3b shows that although the salt concentration is increased by one order of magnitude (from $\rho_s\sigma^3 = 10^{-4}$ to 10^{-3}), the change in the distributions of polyion segments and counterions is very small. The salt concentration is increased mostly outside the brush. The invariance of the PEB structure explains why the brush thickness is insensitive to changes in the low salt concentrations. As shown in Figure 3a, the counterions are mostly trapped within the brush but the long tail distributions of counterions and co-ions suggest that the electrostatic potential is nonzero at the boundary of the polyelectrolyte brush. In the osmotic-brush regime as shown in Figure 3, parts a and b, the salt concentration within the brush is significantly lower than that of the neutralizing counterions, which are mainly trapped in the brush layer. In this case, there are two opposite effects in determining the brush thickness. On one hand, both the osmotic pressure of the counterions and the electrostatic repulsion between unscreened monomers contribute to the expansion of the polyelectrolyte chains;[42] on the other hand, the chain elasticity disfavors the stretch. Because the amount of couterions in the brush layer depends on the graft density of polyelectrolytes, the brush thickness exhibits no noticeable change with the salt concentration.

When the salt concentration is further increased to $\rho_s\sigma^3 = 10^{-2}$, however, Figure 3c shows that there are a significant amount of co-ions within the polyelectrolyte brush. Correspondingly, the concentration of counterions within the brush is also increased. In this case, the distributions of counterions and co-ions resemble those in an electric double layer. Unlike that at low salt concentration, the electrostatic potential essentially disappears at the edge of the salted tethered polyions due to strong screening. In addition, the nonuniform distribution of co-ions suggests a smooth variance of the electrostatic potential within the brush and the imbalance of the local charges.

Figure 3d shows the density profiles in the salted-brush regime. As hypothesized in the scaling analyses,[10] in this regime the salt concentration outside the brush is comparable to that inside. Because of the excluded-volume effects, significant accumulations of both counterions and co-ions are observed near the tethering surface. The addition of salt ions reduces the difference in the osmotic pressure between the brush layer and the bulk solution, and thereby diminishing the driving forces to stretch the polymer chains. As a result, the increase of salt concentration leads to the shrink of PEBs. At high salt concentration, there is essentially no difference in osmotic pressure inside and outside PEBs. The swelling of the polyelectrolyte brush becomes similar to that of a neutral brush. As shown in Figure 3c, the electrostatic neutrality is satisfied at the boundary of the PEB but the nonuniform distribution of co-ions suggests that within the polyelectrolyte brush, the polyions and counterions do not have the same charge distribution.

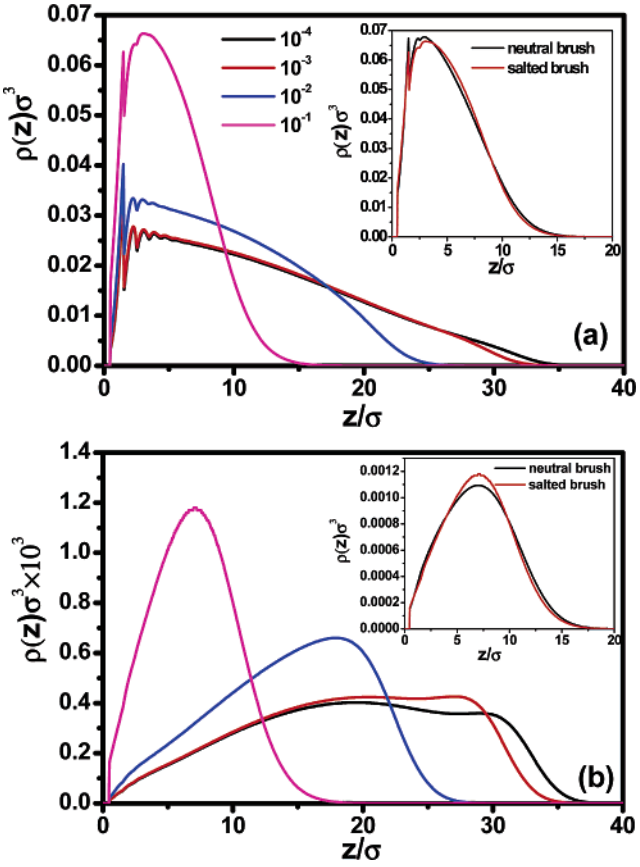

Figure 4. Total (a) and end-segment (b) density profiles for polyions ($M = 50$) at salt concentration $\rho_s\sigma^3 = 10^{-4}$, 10^{-3}, 10^{-2}, 10^{-1}. The grafting density is the same as that appeared in Figure 2. Insets: total (a) and end-segment (b) density profiles of a neutral polymer brush and a salted polyelectrolyte brush at $\rho_s\sigma^3 = 10^{-1}$.

Parts a and b of Figure 4 compare, respectively, the total and end-segment density profiles at different salt concentrations for those systems discussed in Figure 3. Except near the edges, these two set of density profiles are quite different: the total segment density shows an accumulation near the wall but the end segments are depleted. As the salt concentration increases from $\rho_s\sigma^3 = 10^{-4}$ to 10^{-1}, the contraction of the PEB is evident from the receding of the brush rim accompanied by an increase of the overall segment density near the surface. As mentioned earlier, except near the brush boundary, we do not observe much changes in the segment density profiles when the salt concentration is increased from $\rho_s\sigma^3 = 10^{-4}$ to 10^{-3}; in this case, the screening is dominated by counterions. At higher salt concentrations, the PEB shrinks most significantly near the brush edges. Qualitatively, the density profiles shown in Figure 4a are in good agreement with experiments[5] and with molecular simulations.[21]

While the segment density profile defines the brush thickness and PEB structure, the end-segment distribution shown in Figure 4b provides insights into the flexibility of tethered polyions or the softness of PEBs. In comparison to the total segment densities, the end-segment distribution is more sensitive to the change of salt concentration. A broadened end-segment distribution for the swollen brush suggests that the tethered polyions are rather rigid at low salt concentration. At this condition, the inflexibility of polyions arises from the intrachain electrostatic repulsion. Conversely, the Gaussian-like distribution for the brush suggests that at high salt concentration, the tethered polyions are quite flexible.

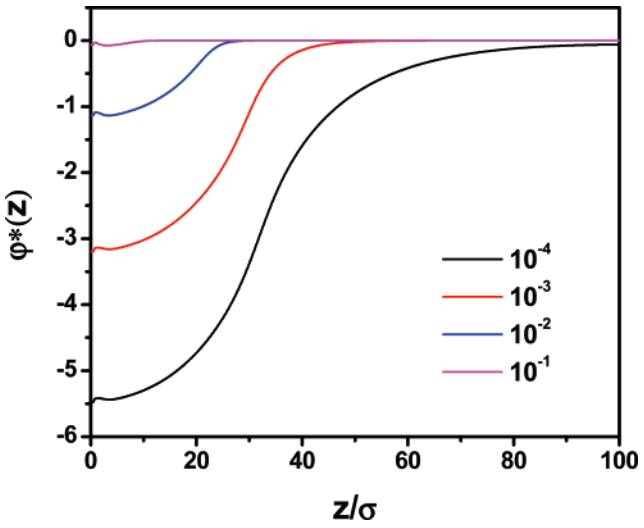

Figure 5. Distributions of the mean electrostatic potentials. All parameters are the same as those used in Figure 4.

In the insets of parts a and b of Figure 4, we show the density profiles of total and end segments for a neutral polymer brush and those for the PEB at the highest salt concentration ($\rho_s\sigma^3 = 10^{-1}$). The two brushes have the same chain length ($M = 50$) and grafting density ($\rho_g\sigma^2 = 10^{-2}$). The neutral brush consists of grafted hard-sphere chains free of intersegment attractions, corresponding to tethered polymers in a good solvent. As expected, the density profiles are nearly identical. For the neutral polymer brush, similar density profiles can be found in previous studies by a mean-field theory[41] and by molecular simulations.[43] For both neutral and salted brushes, the total monomer density profiles are of parabolic shape except some oscillations near the surface. Besides, the end segments are approximately in a Gaussian shape and the chain ends are distributed throughout the entire brush.

Figure 5 shows the variations of the mean electrostatic potentials for systems considered in Figures 3 and 4. In all cases, the mean electrostatic potential exhibits a negative minimum near the tethering surface and rises monotonically to zero in the bulk solution. A small kink close to the surface is induced by the charges of the grafted segments. Because the surface is neutral by itself, the negative mean electrostatic potential is mainly due to the presence of the tethered polyions. Except at the highest salt concentration ($\rho_s\sigma^3 = 0.1$), the negative electrostatic potential extends way beyond the brush boundary for all other cases. Figure 5 indicates that at low salt concentration, a highly charged polyelectrolyte brush behaves much like a charge surface.

3.2. Effect of the Chain Length on Brush Thickness. We studied the variance of the brush thickness with the chain length of the tethered polyions at fixed grafting density, $\rho_g\sigma^2 = 10^{-2}$, corresponding to the brush regime. Figure 6 shows that, in good agreement with previous theoretical and experimental investigations,[4,10,39] the brush thickness scales linearly with the chain length in both osmotic and salted-brush regimes. Because of the stronger electrostatic repulsion, the slope of the osmotic brush is larger than that of the salted brush. The trend agrees very well with experiments on PtBS−PSSNa brushes with different chain lengths.[4]

3.3. Effect of the Grafting Density on Brush Thickness. The grafting density of polyions is also an important parameter in determining the properties of PEBs. According to the scaling analysis,[10,11] the brush thickness is invariant to the grafting density for neutralized osmotic brushes, and it scales as $H \propto$

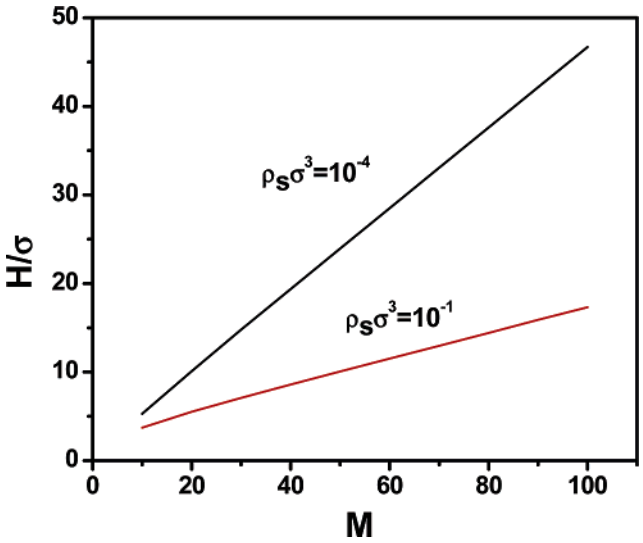

Figure 6. Dependence of the brush thickness on the chain length in the osmotic-brush regime ($\rho_s\sigma^3 = 10^{-4}$) and in the salted-brush regime ($\rho_s\sigma^3 = 10^{-1}$). Here the reduced grafting density is $\rho_g\sigma^2 = 10^{-2}$.

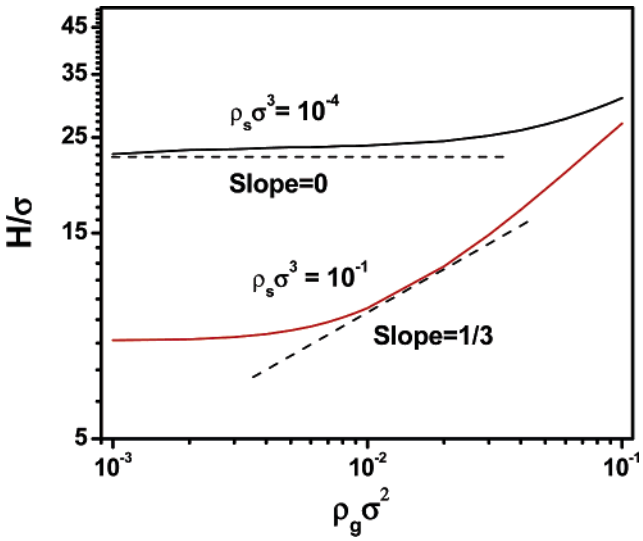

Figure 7. Dependence of the brush thickness on the grafting density in the osmotic-brush regime ($\rho_s\sigma^3 = 10^{-4}$) and in the salted-brush regime ($\rho_s\sigma^3 = 10^{-1}$). Here the chain length is $M = 50$; dashed lines are the predictions of scaling law.

$\rho_g^{1/3}$ for salted brushes. Recent simulations and experiments suggest that even for osmotic brushes, the thickness increases slightly with the grafting density.[5,19,20]

Figure 7 shows the brush thickness as a function of the surface grafting density at two salt concentrations corresponding to the osmotic and salted regimes. In the osmotic-brush regime ($\rho_s\sigma^3 = 10^{-4}$), the brush thickness is relatively insensitive to the grafting density. Nevertheless, it increases slightly from 22.87σ to 30.88σ when the grafting density is increased by 2 orders of magnitude. Although the change is small, apparently the brush thickness is not a constant. The DFT predictions appear in good agreement with recent experiments[5,19] and with other theoretical calculations.[19,20] In the osmotic regime, the counterion density increases with the grafting density of polyelectrolytes. As a result, an increase in the grafting density leads to a higher osmotic pressure and larger brush thickness. The "nonlinear osmotic brush regime" is captured by a mean-field theory that accounts for the excluded-volume interactions between polyelectrolyte segments and small ions.[19] Unlike the mean-field predictions, however, Figure 7 shows that the slope also varies

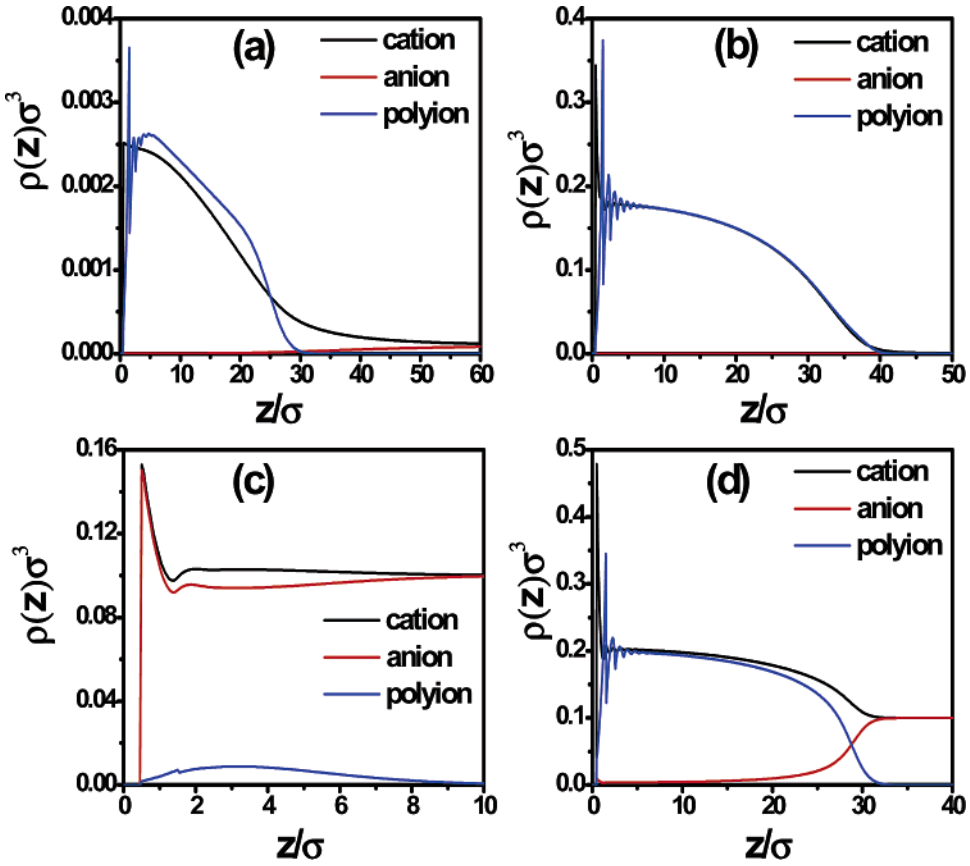

Figure 8. Density profiles of polyions ($M = 50$), cations and anions: (a) $\rho_s\sigma^3 = 10^{-4}$, $\rho_g\sigma^2 = 10^{-3}$; (b) $\rho_s\sigma^3 = 10^{-4}$, $\rho_g\sigma^2 = 10^{-1}$; (c) $\rho_s\sigma^3 = 10^{-1}$, $\rho_g\sigma^2 = 10^{-3}$; (d) $\rho_s\sigma^3 = 10^{-1}$, $\rho_g\sigma^2 = 10^{-1}$. Parts a and b are in the osmotic-brush regime; Parts c and d are in the salted-brush regime.

with the grafting density, implying that in the osmotic regime, there is no simple scaling relation between the grafting density and the brush thickness.[5] In the salted-brush regime, the brush thickness varies little with the grafting density before the overlap of tethered polyions, and it exhibits a quasi-power-law behavior at higher grafting densities that shows stronger dependence on the tethering density in comparison with the scaling analyses and experiments ($H \propto \rho_g^{1/3}$).[4,10,14]

Figure 8 presents the density profiles of the polyion segments and salt ions for the osmotic ($\rho_s\sigma^3 = 10^{-4}$) and salted ($\rho_s\sigma^3 = 10^{-1}$) brushes at two extreme grafting densities ($\rho_g\sigma^2 = 10^{-3}$ and $\rho_g\sigma^2 = 10^{-1}$). Similar densities profiles for an intermediate grafting density ($\rho_g\sigma^2 = 10^{-2}$ and different salt concentrations) are displayed in Figure 3. In both figures, the parameters are the same as those considered in Figure 7. Figure 8a shows that the density profiles of the counterions and co-ions in a sparsely tethered osmotic brush. In this case, the difference in ion densities remains significantly different beyond the brush boundary, suggesting that the brush is not neutralized. Such difference is not shown in Figure 8b because in this case ($\rho_s\sigma^3 = 10^{-4}$, $\rho_g\sigma^2 = 10^{-1}$), the counterion concentration is higher than the salt concentration by several orders of magnitude.

In the salted-brush regime, the electrostatic interactions between polyions are screened by counterions and the PEB shrinks at low grafting density and swells at high grafting density. In this case, the swelling is primarily driven by the strong excluded-volume effects among polymer segments. Figure 8c shows that at low grafting density, the polyelectrolyte chains are essentially isolated and are slightly depleted from the surface due to the accumulation of small ions. The distributions of counterions and co-ions resemble those of hard spheres near a hard wall.[28] At the high grafting density, conversely, the polyions are highly extended and the segment density is approximately uniform, much like that for a neutral brush.

Figure 9 shows the effect of grafting density on the mean electrostatic potential in both osmotic and salted regimes. In the osmotic-brush regime (Figure 9a), the mean electrostatic potential becomes more negative and extends much beyond the brush boundary as the grafting density increases. On the contrary, in salted brushes (Figure 9b), the mean-electrostatic potential becomes essentially zero at the brush boundary. At low grafting density ($\rho_g\sigma^2 = 10^{-3}$) and high salt concentration ($\rho_s\sigma^3 = 10^{-1}$), the mean-electrostatic potential is almost everywhere zero. Figure 9 also suggests that as the grafting density increase, the mean electrostatic potential becomes more sensitive to the salt concentration.

4. Conclusions

Thanks to a number of pervious theoretical investigations and experiments,[4,10,11,14,39] it is fair to state that at least for systems containing monovalent ions, both the swelling behavior and the brush structure of polyelectrolyte brushes are relatively well understood. Less is known though on the specific distributions of small ions and the mean-electrostatic potential profiles with the PEBs. As stated in the introduction, one main purpose of this work is to fill the gap between simulations and scaling analysis, the former is most useful for short chains and the later is for long chains, respectively. On the basis of the above discussions, it appears that the nonlocal density functional theory (DFT) introduced in this work is adequate for that purpose.

We have demonstrated that the DFT is able to capture the effects of salt concentration, chain length and grafting density on PEB properties in good agreement with simulations and with

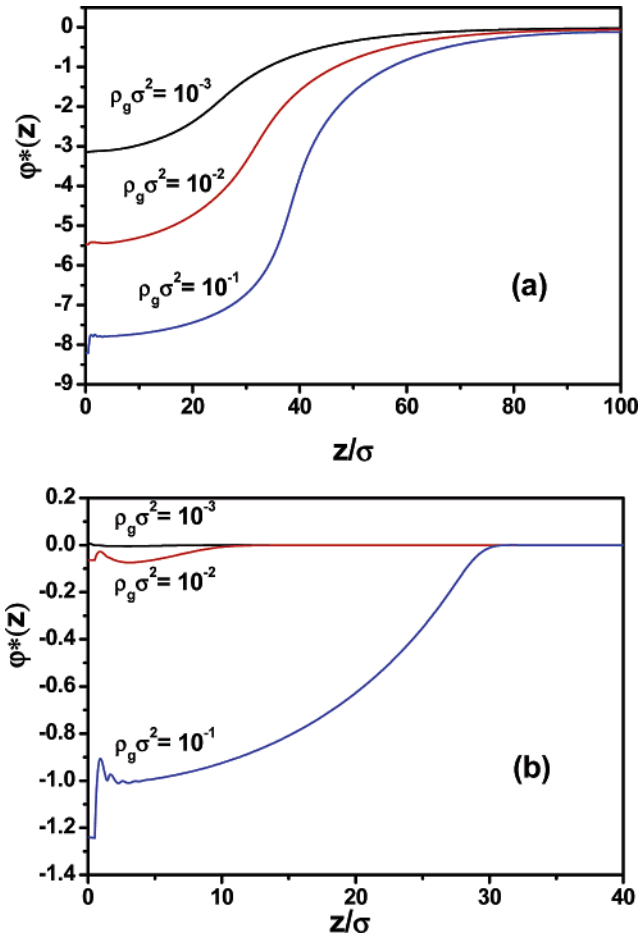

Figure 9. Distributions of the mean electrostatic potentials at salt concentration (a) $\rho_s\sigma^3 = 10^{-4}$ and (b) $\rho_s\sigma^3 = 10^{-1}$. All parameters are the same as those used in Figure 8.

experiments. In comparison with alternative approaches, one important advantage of DFT is that it is equally applicable to different regions of the polyelectrolyte systems, and thereby providing a unifying procedure for predicting the swelling behavior. With the increase in the salt concentration, we are able to identify the transition from an osmotic-brush regime to a salted-brush regime as first defined by Pincus and others.[10,11] Because the swelling of polyions is dictated by the counterions, the thickness of an osmotic brush is relatively insensitive to the salt concentration. In the salted-brush regime, however, the brush thickness falls in a power-law relation at high salt concentrations. In this case, the brush thickness follows the scaling relation $H \propto \rho_s^{-1/3}$ for polyions of sufficiently long chain length ($M \geq 50$). As found in experiments and simulations, the exponent of the power law decreases slightly with the chain length and a different scaling law emerges for sparsely tethered polyelectrolytes or for short-chain polyions.

The DFT calculations allow us to analyze the density distributions of polyion segments and salt ions as well as the mean electrostatic potentials in details. While the former define the brush thickness and microscopic structure, the latter provide insights into the charge distributions beyond the PEB boundary. Besides, the segment density profiles can be used to estimate the magnitude of polyion stretching and the brush softness. By considering the distributions of the salt ions explicitly, we are able to study the characteristics of the osmotic and salted-brush regimes at both low and high concentrations. In the osmotic-brush regime, the density of counterions follows closely that of the segments of the extended polyions. In this case, the effect of salt concentration is negligible because within the brush, the salt ion concentration is much smaller than the counterion concentration. Whereas in the salted-brush regime, the electrostatic interactions are screened by the added salt and the salt concentrations inside and outside the brushes are comparable. In this case, the interaction between polyion segments is dominated by the excluded volume effect, which is sensitive to the salt concentrations. In the osmotic-brush regime, the mean electrostatic potential often extends far beyond the brush boundary, implying the diffusion of counterions into the bulk solution. For a salted brush, the mean electrostatic potential is almost everywhere neutral. As a result, the shrink of a salted brush at high salt concentration is primarily driven by the excluded-volume effect, much like that for a neutral brush.

In good agreement with previous investigations, the brush thickness increases linearly with the chain length in both osmotic and salted-brush regimes. Because of different driving forces, the slope in the salted-brush regime is larger than that in the osmotic-brush regime. We have also examined the influences of the grafting density on the brush swellings, on salt ions distributions, and on variation of the mean electrostatic potentials in both osmotic and salted brush regimes. In consistent with recent experiments and other theoretical investigations, the thickness of an osmotic brush rises noticeably with the grafting density. The thickness of a salted brush increases monotonically with the grafting density but the slope is not a constant as predicted by the scaling analyses.

The main purpose of this work is again to provide a coherent description of the polyelectrolyte brush in terms of a number of important parameters that have been separately studied by previous theoretical analysis, simulations and experiments. The emphasis was placed on the qualitative behavior of swelling instead of quantitative reproduction of simulation or experimental results by fitting the model parameters. Nevertheless, quantitative agreements with experiments and simulations have been identified in terms of the scaling relations. In particular, our DFT calculations yield the power-law dependences of the brush thickness on the salt concentration, grafting density and chain length all in good agreement with recent simulations and experiments. In the future work, we will explore quantitative representations of the experimental data by using more realistic parameters for polymers and salt ions.

Acknowledgment. J.W. is grateful to Matt Tirrell for inspiring discussions. This research used resources of the National Energy Research Scientific Computing Center, which is supported by the Office of Science of the U.S. Department of Energy under Contract No. DE-AC03-76SF00098.

References and Notes

(1) Ruhe, J.; Ballauff, M.; Biesalski, M.; Dziezok, P.; Grohn, F.; Johannsmann, D.; Houbenov, N.; Hugenberg, N.; Konradi, R.; Minko, S.; Motornov, M.; Netz, R. R.; Schmidt, M.; Seidel, C.; Stamm, M.; Stephan, T.; Usov, D.; Zhang, H. N. *Adv. Polym. Sci.* **2004**, *165*, 79−150.
(2) Guenoun, P.; Argillier, J. F.; Tirrell, M. *C. R. Acad. Sci., Ser. IV: Phys. Astrophys.* **2000**, *1*, 1163−1169.
(3) Mir, Y.; Auroy, P.; Auvray, L. *Phys. Rev. Lett.* **1995**, *75*, 2863−2866.
(4) Balastre, M.; Li, F.; Schorr, P.; Yang, J. C.; Mays, J. W.; Tirrell, M. V. *Macromolecules* **2002**, *35*, 9480−9486.
(5) Romet-Lemonne, G.; Daillant, J.; Guenoun, P.; Yang, J.; Mays, J. W. *Phys. Rev. Lett.* **2004**, *93*, Art. No. 148301.
(6) Napper, D. H. *Polymeric Stabilization of Colloidal Dispersions*; Academic Press: London, 1983.
(7) Wittemann, A.; Haupt, B.; Ballauff, M. *Phys. Chem. Chem. Phys.* **2003**, *5*, 1671−1677.
(8) Pavoor, P. V.; Gearing, B. P.; Bellare, A.; Cohen, R. E. *Wear* **2004**, *256*, 1196−1207.

(9) Klein, J.; Kamiyama, Y.; Yoshizawa, H.; Israelachvili, J. N.; Fredrickson, G. H.; Pincus, P.; Fetters, L. J. *Macromolecules* **1993**, *26*, 5552−5560.
(10) Pincus, P. *Macromolecules* **1991**, *24*, 2912−2919.
(11) Borisov, O. V.; Birshtein, T. M.; Zhulina, E. B. *J. Phys. II* **1991**, *1*, 521−526.
(12) Misra, S.; Tirrell, M.; Mattice, W. *Macromolecules* **1996**, *29*, 6056−6060.
(13) Guenoun, P.; Muller, F.; Delsanti, M.; Auvray, L.; Chen, Y. J.; Mays, J. W.; Tirrell, M. *Phys. Rev. Lett.* **1998**, *81*, 3872−3875.
(14) Tamashiro, M. N.; Hernandez-Zapata, E.; Schorr, P. A.; Balastre, M.; Tirrell, M.; Pincus, P. *J. Chem. Phys.* **2001**, *115*, 1960−1969.
(15) Ross, R. S.; Pincus, P. *Macromolecules* **1992**, *25*, 2177−2183.
(16) Zhulina, E. B.; Borisov, O. V.; Birshtein, T. M. *J. Phys. II* **1992**, *2*, 63−74.
(17) Borisov, O. V.; Zhulina, E. B.; Birshtein, T. M. *Macromolecules* **1994**, *27*, 4795−4803.
(18) Zhulina, E. B.; Birshtein, T. M.; Borisov, O. V. *Macromolecules* **1995**, *28*, 1491−1499.
(19) Ahrens, H.; Forster, S.; Hehn, C. A.; Kumar, N. A.; Naji, A.; Netz, R. R.; Seidel, C. *J. Phys. Chem. B* **2004**, *108*, 16870−16876.
(20) Naji, A.; Netz, R. R.; Seidel, C. *Eur. Phys. J. E* **2003**, *12*, 223−237.
(21) Kumar, N. A.; Seidel, C. *Macromolecules* **2005**, *38*, 9341−9350.
(22) Chen, H.; Zajac, R.; Chakrabarti, A. *J. Chem. Phys.* **1996**, *104*, 1579−1588.
(23) Hehmeyer, O. J.; Panagiotopoulos, A. Z. Private communication.
(24) Wu, J. Z. *AIChE J.* **2006**, *52*, 1169−1193.
(25) Wu, J.; Li, Z. *Annu. Rev. Phys. Chem.* **2007**, *58*, 85−112.
(26) Li, Z. D.; Wu, J. Z. *J. Phys. Chem. B* **2006**, *110*, 7473−7484.
(27) Li, Z. D.; Wu, J. Z. *Phys. Rev. Lett.* **2006**, *96*, 048302.
(28) Yu, Y. X.; Wu, J. Z. *J. Chem. Phys.* **2002**, *117*, 10156−10164.
(29) Roth, R.; Evans, R.; Lang, A.; Kahl, G. *J. Phys.-Condens. Matter* **2002**, *14*, 12063−12078.
(30) Rosenfeld, Y. *Phys. Rev. Lett.* **1989**, *63*, 980 - 983.
(31) Yu, Y. X.; Wu, J. Z. *J. Chem. Phys.* **2002**, *117*, 2368−2376.
(32) Jiang, J. W.; Liu, H. L.; Hu, Y.; Prausnitz, J. M. *J. Chem. Phys.* **1998**, *108*, 780−784.
(33) Jiang, J. W.; Blum, L.; Bernard, O.; Prausnitz, J. M. *Mol. Phys.* **2001**, *99*, 1121−1128.
(34) Yu, Y. X.; Wu, J. Z.; Gao, G. H. *J. Chem. Phys.* **2004**, *120*, 7223−7233.
(35) Blum, L. *Mol. Phys.* **1975**, *30*, 1529−1535.
(36) Hoye, J. S.; Blum, L. *Mol. Phys.* **1978**, *35*, 299−300.
(37) Fredrickson, G. H. *The Equilibrium Theory of Inhomogeneous Polymers*; Oxford University Press: New York, 2006.
(38) Patra, C. N.; Chang, R.; Yethiraj, A. *J. Phys. Chem. B* **2004**, *108*, 9126−9132.
(39) Li, F.; Balastre, M.; Schorr, P.; Argillier, J. F.; Yang, J. C.; Mays, J. W.; Tirrell, M. *Langmuir* **2006**, *22*, 4084−4091.
(40) Auroy, P.; Auvray, L.; Leger, L. *Phys. Rev. Lett.* **1991**, *66*, 719−722.
(41) Zhulina, E. B.; Borisov, O. V.; Pryamitsyn, V. A.; Birshtein, T. M. *Macromolecules* **1991**, *24*, 140−149.
(42) Roger, M.; Guenoun, P.; Muller, F.; Belloni, L.; Delsanti, M. *Eur. Phys. J. E* **2002**, *9*, 313−326.
(43) Seidel, C.; Netz, R. R. *Macromolecules* **2000**, *33*, 634−640.

MA061939T